

# **Linking Extratropical Forecast Degradation to Tropical Cyclones in Physical and AI Models**

**Gan Zhang<sup>1\*</sup>**

<sup>1</sup> Department of Climate, Meteorology & Atmospheric Sciences, University of Illinois Urbana-Champaign, Urbana, Illinois

\*Corresponding Author: Gan Zhang (gzhang13@illinois.edu)

## Key Findings

- Tropical cyclones can lead to severe skill degradation in Week-2 extratropical forecasts on regional (e.g., Europe) and global scales.
- Besides recurring cyclones, zonally-moving cyclones in the tropics can contribute to Rossby wave responses and large extratropical errors.
- Initialized near tropical cyclogenesis, physical and AI-hybrid models make comparable predictions of extratropical geopotential height.

## Abstract

Global medium-range weather forecasts suffer occasional failures ("busts"), often linked to tropical cyclones (TCs). We systematically investigate the TC influences by clustering historical TC tracks and comparing skill of forecasts from a physics-based model (ECMWF-IFS) and an AI-physics hybrid model (Google-NGCM) initialized near TC genesis. Case analysis shows both models exhibit similar large-scale error growth in the extratropics, suggesting prediction skill bounded by similar limits despite model differences in spatial resolution and parameterized physics. Aggregated statistics reveal that low skill of Week-2 forecasts may occur after TC genesis, regardless of whether they recurve or not. While recurring tracks are established error sources, zonal-track clusters can be associated with similarly profound forecast degradation, acting through Rossby wave dynamics and remote moisture transport mechanisms. Furthermore, the stochastic

NGCM generally outperforms its deterministic counterpart and suggests that TC-related forecast degradation is more pronounced for Europe than elsewhere in the Northern Hemisphere.

### **Plain Language Summary**

Even with substantial progress in recent decades, weather forecasts sometimes go significantly wrong when looking one to two weeks ahead. These "forecast busts" can happen when hurricanes or typhoons (namely tropical cyclones) are present. Our research mapped out the common paths these storms take using historical data. We then compared forecasts made by a physics-based, fine-resolution weather model with a faster, coarse-resolution AI weather model and initialized when the storms first formed. Both models struggled with similar storm patterns, suggesting these errors stem from the atmosphere's inherent unpredictability rather than model flaws. Crucially, while northward-curving storms are known to disrupt forecasts, we discovered that storms traveling mostly westward (zonal tracks) can also cause severe errors in distant regions, likely by exciting upper-tropospheric waves and transporting moisture that destabilizes the atmosphere. The AI model performed significantly better when it included "randomness" to represent uncertainty, and experiments with the AI model suggested that Europe tends to experience poorer forecasts.

## 1. Introduction

The numerical weather prediction (NWP) has been one of the great scientific achievements of the last century (Bauer et al., 2015). Predictions of large-scale weather patterns are now routinely skillful out to two weeks or more, assisting emergency management, energy forecasting, agriculture planning, and other weather-sensitive applications. Despite this progress, these predictions are still prone to occasional but significant failures, known as "forecast busts", where the forecast rapidly deviates from the observed atmospheric evolution (Rodwell et al., 2013). Understanding the precursors and dynamics driving these busts is crucial for improving forecast reliability and potentially extending the horizon of useful weather predictions.

Studies investigating forecast busts, often focusing on verification over Europe, have revealed strong connections with upstream meteorological precursors. Rodwell et al. (2013) analyzed forecast bust cases and suggested that the springtime busts for Week-1 prediction are associated with mesoscale convective systems (MCSs) developing over North America. Supported by low-level moisture transport from the US South and Gulf of Mexico, the MCSs contribute to Rossby wave trains across the Atlantic and surprises NWP models. Lillo & Parsons (2017) conducted a comprehensive study of 584 forecast busts for 6-day predictions verified over Europe. The work revealed a prominent seasonal peak of forecast busts in September and October, a period that coincides with the peak of the Atlantic hurricane season and spawns recurring tropical cyclones (TCs). This finding pointed towards a strong, though not exclusive, link between TC activity and Week-1 forecast busts.

The basic physical mechanism linking recurring TCs to downstream forecast error is conceptually well-understood and supported by modeling studies (Keller et al., 2019). As a TC

moves poleward and interacts with the mid-latitude jet stream, it can undergo extratropical transition (ET) (Evans et al., 2017). Nonlinear, large-amplitude flow disturbances can arise when TCs recurve in the Northwestern Pacific (e.g., Archambault et al., 2013) and the North Atlantic (e.g., Brannan & Chagnon, 2020). The trajectory of a recurring TC and subsequent flow evolution are sensitive to the phasing of the TC tracks and midlatitude waves (Riboldi et al., 2019; Riemer & Jones, 2014). The diabatic heating and potential vorticity (PV) anomalies associated with the recurring cyclone can perturb the midlatitude jets (Archambault et al., 2015; Evans et al., 2017), radiating Rossby wave trains that propagate downstream (Archambault et al., 2013; Keller et al., 2019; Quinting & Jones, 2016). In some cases, amplifying ridges and troughs alter the large-scale flow pattern thousands of kilometers away, leading to high-impact weather (e.g., Pohorsky et al., 2019; Riboldi et al., 2019) or a rapid decrease in forecast skill (Aiyer, 2015; Quinting & Jones, 2016; Harr & Archambault, 2017). While the downstream impact is highly dependent on the TC genesis location and subsequent track (Grams & Archambault, 2016; Keller et al., 2019), TC intensity has been shown to have relatively small impact on downstream wave characteristics (Riemer & Jones, 2010; Archambault et al., 2013; Riboldi et al., 2019).

Meanwhile, increasing evidence suggests potential impacts of TCs on extratropical forecasts are not limited to recurring cases. Recent observational evidence suggests that TC recurring is not a necessary condition for the excitation or amplification of midlatitude Rossby waves (Sinclair, 2025). Even when residing in the tropics, TCs can interact with equatorward intruding midlatitude waves (Zhang et al., 2016, 2017), and the diabatic outflow from TCs may lead to amplified Rossby wave responses (Grams & Archambault, 2016). Furthermore, such interactions can export tropical moisture from the vicinity of TCs to higher latitudes, which can result in extremes such as predecessor rain events (Cordeira et al., 2013; Galarneau et al., 2010).

Understanding TC-induced forecast busts has traditionally been challenging. Past studies of the impacts of recurring TCs on downstream weather predictability often rely on NWP case simulations (Riemer & Jones, 2014; Grams & Archambault, 2016), which are often limited by the computational expense of running large-ensemble simulations needed to robustly study high-impact, relatively infrequent events. Some studies analyzed archived operational forecasts (Aiyer, 2015; Anwender et al., 2008) but were limited to a small sample size due to frequent updates of operational NWP models. Recent studies leverage reforecasts generated by model developers (Harr & Archambault, 2017; Quinting & Jones, 2016) but are limited by the relatively sparse initialization time, which leaves out many TC cases. Finally, past predictability studies of forecast busts mostly focus on Week-1 forecasts initialized around TC recurring (e.g., Lillo & Parsons, 2017), leaving long-range prediction and the impacts of early-stage TC development understudied.

The recent advance of Artificial Intelligence (AI) offers a transformative tool for weather forecasting (e.g., Bi et al., 2023; Lam et al., 2023; Price et al., 2023; Kochkov et al., 2024; Bonev et al., 2025). These data-driven models can produce forecasts orders of magnitude faster than traditional NWP models, enabling large-scale experimentation that would otherwise be cost-prohibitive. Among these, the Neural General Circulation Model (NGCM) is a hybrid model combining a numerical dynamical core with machine-learned parameterizations for physical processes like radiation and turbulence (Kochkov et al., 2024). The NGCM has delivered skillful two-week prediction of global weather (Kochkov et al., 2024) and subseasonal-to-seasonal prediction of TC activity (Zhang et al., 2025). These traits make the NGCM well positioned to enable comprehensive experimentation investigating TC-induced extratropical forecast busts.

A comparative study with physical and AI models may help alleviate key limitations of past research and reveal new research opportunities. As AI models mature and enter operation, this

presents a unique opportunity to compare the behavior of these two distinct modeling paradigms in highly challenging forecast scenarios. Furthermore, while the current AI models capture the large-scale tropospheric weather dynamics (e.g., Chen et al., 2025; Hakim & Masanam, 2023), they mostly operate at significantly coarser resolutions than state-of-the-art physical forecasting systems ( $\sim 0.1^\circ$  grid spacing). These low-resolution AI models thus cannot explicitly resolve the storm's internal structure or the detailed physics of extratropical transition. This presents a key question: Can a lower-resolution AI model—trained with proper uncertainty representation—adequately capture the downstream large-scale impacts and forecast busts originating from TCs?

This study conducts a comparative forecast analysis of TC track clusters and extratropical impact regions. Using a high-resolution physical model (ECMWF-IFS) and a lower-resolution AI model (NGCM), we investigate:

1. How may TC track archetypes be linked to extratropical skill degradation extending into Week-2 forecasts?
2. Does the lower-resolution NGCM capture the impacts of TCs on extratropical forecasts similarly as the high-resolution IFS?

By analyzing ensemble forecasts initialized near TC genesis, we characterize the connection between TCs and extratropical predictability loss in physical and AI models. This comparison illuminates the capabilities of AI weather models and offers insights relevant to both operational forecasting and ongoing model development.

## 2. Data and Methods

### 2.1 Tropical Cyclone Tracks and Clustering

Historical atmospheric states and TC tracks of 1979–2022 were sourced from the European Centre for Medium-Range Weather Forecasts (ECMWF) reanalysis version 5 (ERA5) dataset (Hersbach et al., 2020). Specifically, the ERA5 tracks used here were identified by Han & Ullrich (2025) using the TempestExtreme package . The tracking algorithm objectively detects and tracks cyclone features based on sea-level pressure minima, wind speed thresholds, and warm-core characteristics. Furthermore, the extratropical transition is determined using threshold checks of average deep-layer wind shear and maximum stratosphere relative humidity near storms (Han & Ullrich, 2025). While best track datasets (e.g., IBTrACS; Knapp et al., 2010) represent official TC analyses, this study chooses ERA5 tracks primarily to ensure consistency between the TC data and the ERA5 data used for initializing the NGCM forecasts. Furthermore, using a single, globally consistent dataset avoids potential inhomogeneities between different agencies' operational practices. Even though TC detection and intensity in reanalyses can be resolution-dependent and may exhibit biases, these tracks are generally consistent with best track data, especially for stronger storms (Han & Ullrich, 2025; Hodges et al., 2017).

Focusing on TCs developing in July–November, we applied a clustering algorithm to the ERA5 track data for the North Atlantic (NA), Eastern Pacific (EP), and Western Pacific (WP) basins. The goal of this procedure is to group cyclones that share similar spatial characteristics in their genesis location and subsequent trajectory. To prepare the tracks for clustering, we apply a trajectory clustering algorithm (TRACLUS) (Lee et al., 2007) which segments each trajectory based on its geometric properties, effectively creating a standardized vector representation. We then apply K-

means algorithm to these trajectory representations group similar tracks. The resulting clusters were labeled a, b, c, and d within each basin, arranged geographically from west (a) to east (d). This objective classification helps systematically associate forecast outcomes with specific TC behaviors. The choice of  $k=4$  clusters follows previous studies of the North Atlantic (Kossin et al., 2010; Camargo et al., 2021) and considers the balance of representativeness and simplicity. Sensitivity tests and additional discussion are available in Supplementary Materials.

## 2.2 Forecast Models

This study uses two distinct global weather forecast models to represent physical and AI-based prediction.

- **Integrated Forecasting System (IFS):** The IFS is the operational global NWP model developed and maintained by ECMWF. It is a spectral model that solves the primitive equations of atmospheric motion, incorporating a sophisticated suite of physical parameterizations to represent processes like convection, radiation, and turbulence. This study uses a set of IFS forecasts sourced from the THORPEX Interactive Grand Global Ensemble (TIGGE) archive (Bougeault et al., 2010) covering 2020–2022, approximately corresponding to IFS Cycle-47 version. During this period, the IFS ensemble consisted of 50 members, generated using an Ensemble of Data Assimilations (EDA) and singular vector perturbations, running at a horizontal resolution of  $\sim 18$  km.
- **Neural General Circulation Model (NGCM):** The NGCM is an AI-based weather model that employs a numerical dynamical core to resolve atmospheric dynamics but replaces traditional sub-grid physics parameterizations with components learned directly from ERA5 data (Kochkov et al., 2024). The primary advantages of the NGCM are its

computational efficiency and its ability to capture complex non-linear relationships without explicit physical formulation. We analyze ensemble forecasts from the deterministic NGCM and the stochastic NGCM at a horizontal grid spacing of  $\sim$ 1.4 degrees ( $\sim$ 155 km at the equator). The stochastic NGCM includes probabilistic components and was trained with a probabilistic loss function to better represent model uncertainty. Additional details about the ensemble forecast strategy were documented by Kochkov et al. (2024) and Zhang et al. (2025).

Crucially, the two models differ substantially in resolution ( $\sim$ 18 km for IFS vs.  $\sim$ 155 km for NGCM). This large difference in resolution means the NGCM cannot explicitly resolve the fine-scale internal structure of TCs or extratropical transitions in the same way as the IFS. A key focus of the comparison is thus whether the NGCM can capture the downstream, large-scale predictability impacts.

### 2.3 Experiment Design and Evaluation

For each of the track cluster, we generate NGCM forecasts initialized near the genesis time for  $\sim$ 30 most recent TC cases in the ERA5 track dataset (Han & Ullrich, 2025). To keep the data volume of 359 cases manageable, we perform 20-member (instead of 50-member) ensemble prediction with the stochastic and the deterministic NGCM, respectively. In each case, we pair the 20-member NGCM ensembles with the first 20 members from the available IFS ensemble for a fair comparison. For simplicity, forecasts are initialized at 00:00 UTC on the day closest to the time of TC genesis, defined as the first time reaching 34-knot intensity. Different from previous studies that initialize experiments near TC recurving, this initialization strategy characterizes the full potential forecast impacts by the TC, even before the TC's primary interaction with the midlatitude flow.

The model evaluation uses the ERA5 and IFS data that are coarsened to the NGCM grid. Cases are analyzed individually and collectively to detail error evolution in the IFS and the NGCM forecasts. We first analyze two individual cases to demonstrate weather processes, and additional skill analyses examine more cases. The direct skill comparison with the IFS focuses on 102 cases during 2020-2022 to match the forecasts of IFS Cycle-47 version. Furthermore, the 2020-2022 cases occur outside the NGCM training period (1979–2019) and thus serve as out-of-sample validation. The comparison among track clusters uses all the NGCM cases (N=359) to keep the sample size of each track cluster comparable.

Following Rodwell et al. (2013), our skill analysis focuses on the 500-hPa geopotential height (Z500), a key indicator of the large-scale mid-troposphere flow pattern. The consistency between the ensemble means and the ERA5 is evaluated using Root Mean Square Error (RMSE), Anomaly Correlation Coefficient (ACC), and Mean Absolute Error (MAE). We acknowledge that the evaluation here does not fully characterize model performance regarding TCs and other extremes (e.g., surface wind), where coarse-resolution AI models tend to underperform (DeMaria et al., 2025; Pasche et al., 2025). While detailed process-based diagnostics are currently limited by available output variables, the focus on standard skill metrics allows this study to establish a baseline of model and predictability characteristics.

### 3. Results

#### 3.1 Case Study of Forecast Error Growth

To illustrate the synoptic-scale evolution and error growth mechanisms of different TC tracks, we first examine the evolution of 500-hPa geopotential height (Z500) in the ERA5 and the IFS and NGCM forecasts for Hurricane Larry (2021) and Hurricane Laura (2020) (Figure 1). These

two TCs represent zonal and recurving tracks from North Atlantic (Section 3.2), respectively. Before recurving, Hurricane Larry moved northwestward and merged with a tropical moisture plume associated with the residuals of Hurricane Ida (2021) (Figures 1a-b). Wave activity fluxes suggest Hurricane Larry, while still residing in the tropics, contributed to wave development in the East Atlantic (Figure 1d). After recurving, Hurricane Larry interacts with a midlatitude trough and amplifies an atmospheric block pattern, contributing to high-amplitude, localized forecast errors over the Atlantic (Figure 1c). In comparison, Hurricane Laura mostly follows a zonal track before landfall, and its moisture transport feeds into moisture plumes extending towards Europe, which are associated with an extratropical trough intruding into the tropics (not shown) and later the residuals of Hurricane Marco (2020) (Figure 1g). After landfall, wave activity flux suggests Hurricane Laura contributed to the trough development near the US East coast. Furthermore, the residuals of Hurricane Laura feeds moisture to developing troughs near the US east coast, contributing to a propagating wave train that resulted in large forecast errors over the North Atlantic (Figure 1h-i).

Both cases involved tropical moisture transport by a preceding and a developing TC, which collectively contributed to the complex midlatitude flow evolution. While it is hard to attribute the forecast errors to a single source, certain aspects of these cases resemble dynamic pathways documented by previous studies. Specifically, the error growth in Hurricane Larry case appears to have two phases: a Rossby wave responses emanating from the TC when it still resides in the tropics, and the conventional extratropical transition cases, where recurving TCs directly interact with the midlatitude flow. The error growth in Hurricane Laura case involves moisture transport similar to predecessor rain events (Bosart et al., 2012; Galarneau et al., 2010), and the convective triggering of Rossby waves and forecast errors documented by Rodwell et al. (2013).

The error growth patterns in the IFS forecasts and the NGCM forecasts are highly consistent in the two cases, suggesting the NGCM correctly capture the dynamics of complex flow evolutions. For example, the consistency is notable in the case of Hurricane Larry despite the complex flow evolution (Figure 1c vs. 1f). Interestingly, the NGCM forecast errors are smaller than the IFS's, especially for Day-8 forecasts of Hurricane Larry (Figure 1b vs. 1e), suggesting the NGCM performed well despite its low resolution and benefited from the more accurate prediction of the midlatitude flow. Since both hurricane cases occurred after the training period of the NGCM, the consistency here also builds confidence in the out-of-sample performance of NGCM forecasts.

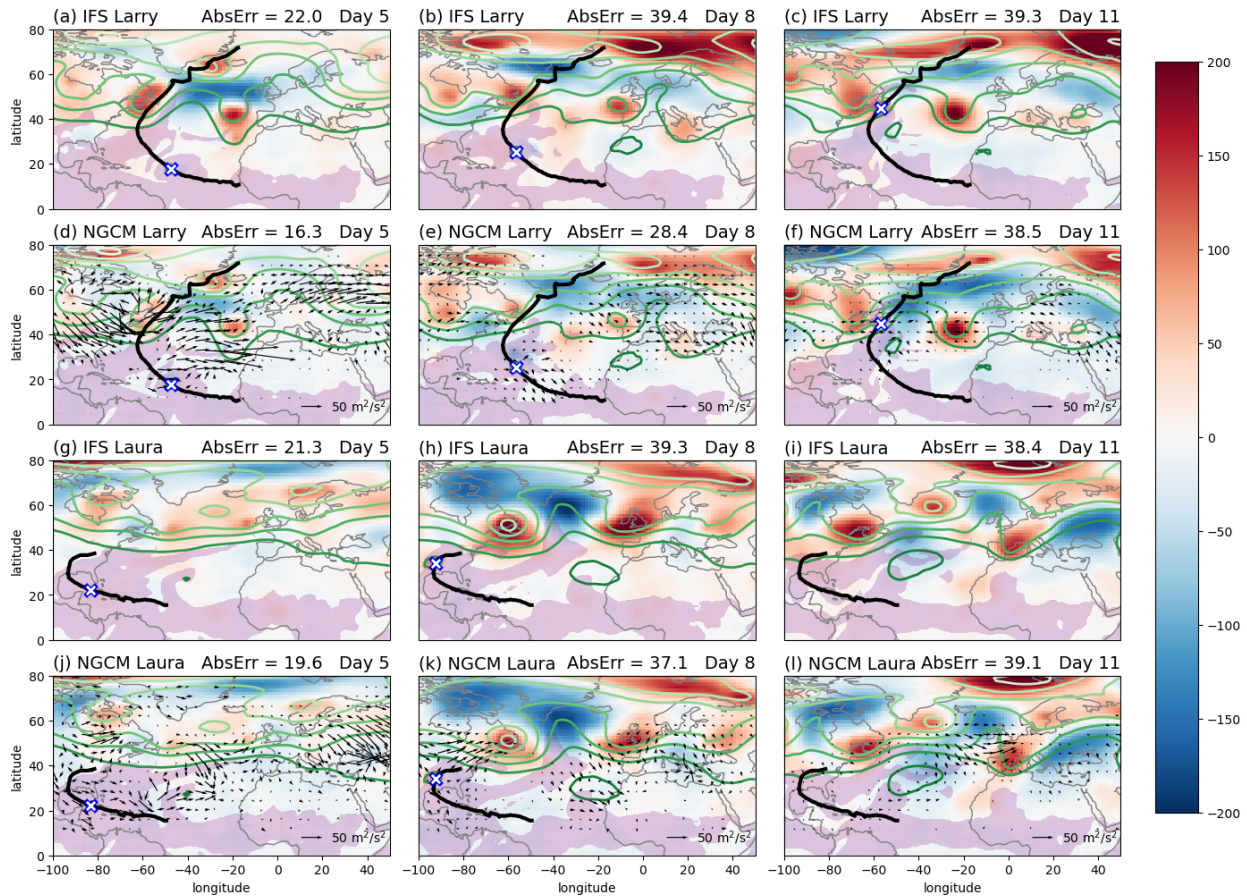


Figure 1: Forecast errors and ERA5 reference for a zonal and a recurving track case in the North Atlantic. The case (a-f) of Hurricane Larry (Cluster d; Section 3.3) is initialized on 2021-08-31,

and the case (g-l) of Hurricane Laura (Cluster c; Section 3.3) is initialized on 2020-08-20. (a) the ERA5 500-hPa geopotential height (Z500) (contour lines, unit: m), Z500 errors of IFS forecasts (20-member) (red-blue shading, unit: m), and storm location (white cross with blue edge) for Day 5 prediction. The black line shows the full TC track, and purple shading highlight areas with total column water vapor  $> 40$  mm. (b)(c) Same as (a), but for Day 8 and Day 11 prediction, respectively. (d-f) Same as (a-c), but for the NGCM forecasts. (g-l) Same as (a-f), but for Hurricane Laura. “AbsErr” in the subplot titles indicates absolute error of forecasts averaged in the plotting domain. The vectors in NGCM panels show the 200-hPa wave activity flux (Takaya & Nakamura, 2001) calculated using the NGCM forecasts, with low values masked out for clarity.

### 3.2 Aggregated Forecast Skill: High-Resolution IFS vs. Low-Resolution NGCM

Moving to the aggregated forecast skill, Figure 2 shows the 15-day evolution of forecast skill as a function of latitude for 102 forecasts initialized near TC genesis. We analyze RMSE and ACCs of a 20-member ensemble of IFS forecasts as the baseline. Both metrics suggest the forecast skill gradually decays as the forecast lead increases. By Day 7 and extending through Week 2, the decay accelerates and becomes more pronounced in the extratropics. Additional spatial details are available in Figure S4. Increasing the ensemble size to 50 members generally reduces RMSE (Figure 2a) and increases ACCs (Figure 2c) moderately, suggesting a larger ensemble size helps mitigate some forecast uncertainty.

Compared to the 20-member IFS forecasts, the NGCM forecasts show regional strengths and weaknesses (Figure 2b and 2d). For example, RMSE of the NGCM forecasts is relatively large near the initialization time and in tropics (Figure 2b). Conversely, the NGCM forecasts show lower RMSE in the extratropics in Week 2. Consistent with the RMSE findings, ACCs suggest that NGCM has a skill deficit in the tropics and a potential extratropical advantage, though many details

depend on forecast time and regions (Figure 2d and S5). The Mean Absolute Error and significant tests (DelSole & Tippett, 2016) suggest the IFS and NGCM perform similarly with extratropical Z500 (Figure S6). We emphasize the performance parity does not necessarily extend to other operationally critical areas, such as forecasting surface wind of TCs (e.g., DeMaria et al., 2025; Zhang et al., 2025).

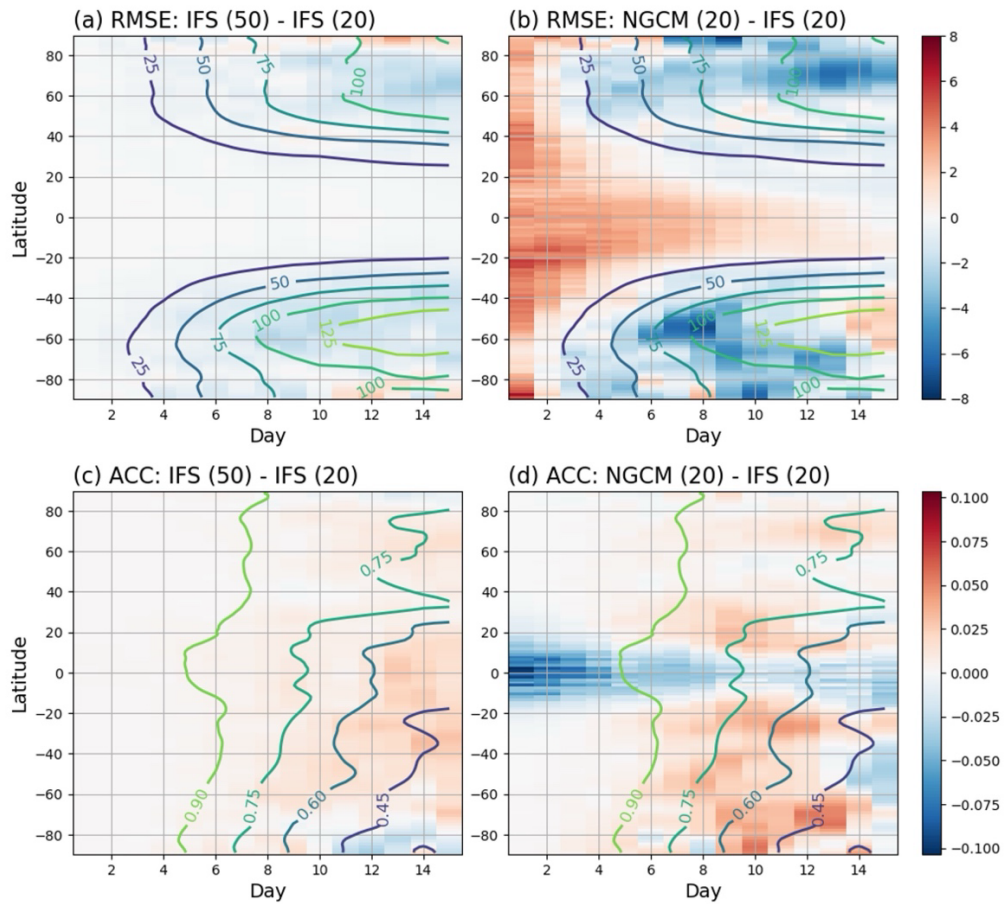


*Figure 2: Comparison of the zonal averages of RMSE and ACCs for 102 cases in 2020-2022. The contours in (a)(b) and (c)(d) show the RSME and the ACCs of a 20-member ensemble of IFS forecasts, respectively, which are calculated for each forecast day and grid point and then averaged zonally. The color shading shows (a) RMSE differences between the 50-member ensemble and a 20-member subset of IFS forecasts, and (b) RMSE differences between a 20-*

*member NGCM stochastic ensemble and a 20-member ensemble of IFS forecasts. (c) Same as (a), but for ACCs. (d) Same as (b), but for ACCs. Lower RMSE and higher ACCs indicate higher forecast skill. The calculations used the anomalies defined using the averages of all the 102 cases for each dataset.*

### 3.3 Characteristics of Tropical Cyclone Track Clusters

The case studies of Larry and Laura suggest that forecast skill degradation is not limited to TC recurring. To investigate how common such degradation is, we apply the objective clustering algorithm described in Section 2.1 to TC tracks and identifies four distinct archetypes in each basin (Figure 3). The track clusters are generally well separated and broadly represent zonal and recurring motion of TCs. For instance, zonal tracks are mostly in WP cluster a, EP cluster b-c, and NA cluster c, while recurring tracks dominate the rest clusters. The tracks strongly affect whether TCs experience the extratropical transition: <50% TCs in the zonal clusters experienced the extratropical transition, while >50% TCs in the recurring clusters underwent the extratropical transition. The recurring, transitioning TCs are the classic storms that were extensively studied for their downstream impacts (e.g., Keller et al. 2019).

Similar tracks have been investigated by previous research in individual basins (e.g., Camargo et al., 2007, 2008; Kossin et al., 2010). For example, Clusters c and d in the North Atlantic are concentrated during August-September, typical of Cape Verde hurricanes; Clusters a and c also peak in late summer but have a broader seasonal distribution (Figure S2). The lifespan of tracks is generally 100-200 hours, with a lifespan up to ~500 hours (Figure S3). Notably, some zonal-motion TCs have a long lifespan (e.g., NA cluster c) in the moist tropical environment, which enable these TCs to fetch and transport a high volume of moisture. The moisture transport induced by TCs is not limited to their vicinity and can reach remote extratropical regions (>1000 km away), as

suggested previous research (Bosart et al., 2012; Cordeira et al., 2013; Galarneau et al., 2010) and case analysis in Section 3.1.

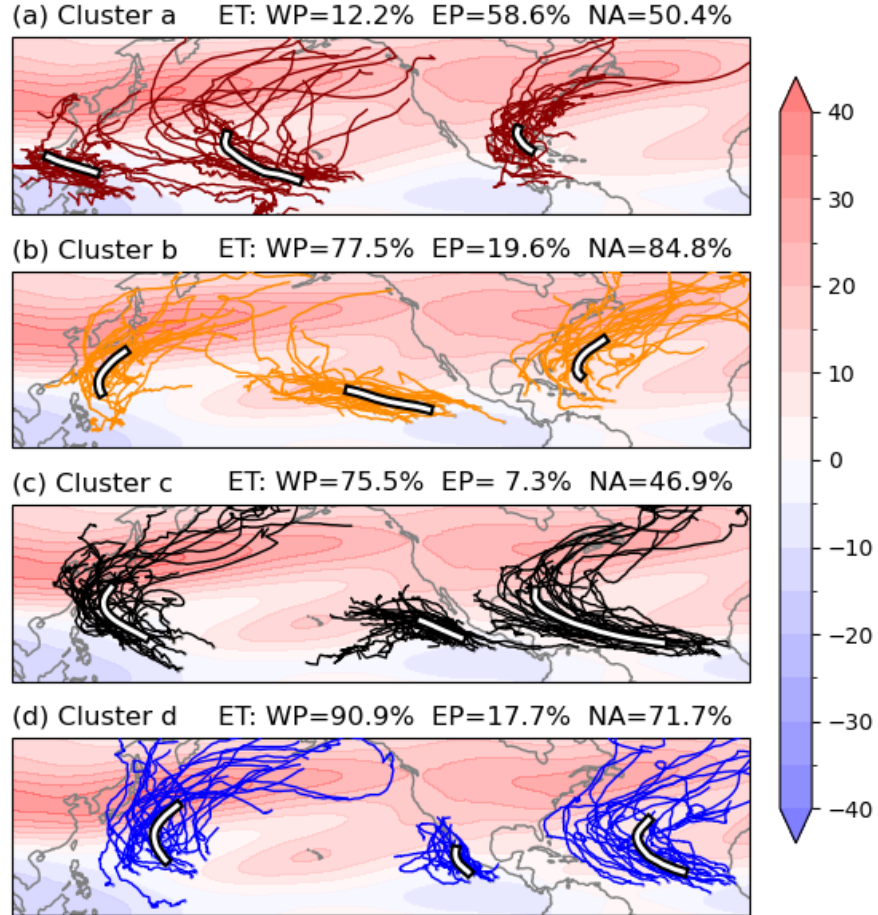


*Figure 3: Spatial characteristics of the TC track clusters and the 200-hPa zonal wind from ERA5 data. (a) Clusters a tracks for all the three basins (NA, EP, and WP). (b)(c)(d) are the same as (a), but for Clusters b, c, and d tracks, respectively. For clarity, each panel displays 30 tracks for all cyclones within clusters, with Cluster a in EP showing 29 cases due to the data availability. Thickened white lines with black edges indicate mean trajectories of all tracks in each cluster. Color shading shows the mean 200-hPa zonal wind (unit:  $m s^{-1}$ ) of June-November of 1990-2019. The ratio of the extratropical transitions for each cluster is denoted at the top right of each panel.*

### 3.4 Prediction Skill by TC Cluster

After establishing the performance baseline of the NGCM, we examine the extratropical flow predictability associated with each track cluster using the NGCM. Compared to the IFS archive, the sample size of NGCM is substantially higher (102 vs 359) and enables more robust skill assessments. Following Rodwell et al. (2013), we discuss forecast busts in the ACC context for Z500 in Europe and US domains (Figure 4). Additional findings about the skill sensitivity to skill metric and model configuration, along results for the Northern Hemisphere extratropics, are available in Supplementary Materials.

TCs in recurring and zonal-motion clusters show similar associations with low-ACC forecasts (Figure 4). Despite a relatively large sample size ( $N \approx 30$ ), the ACC spread in each cluster is substantial in Week 2 and make it hard to identify statistically significant differences. Nonetheless, the results suggest that low-ACC forecasts are not dominated by recurring TCs. Extremely poor forecasts ( $ACC < 0.2$ ) can occur with TCs in nearly every cluster. Despite striking differences in the ratio of extratropical transition (Figure 3), the recurring clusters and the zonal-track clusters show comparable numbers of poor forecasts (Figure 4). We acknowledge that recurring TCs are more capable of contributing to high forecast errors in Europe and the US (Figure S7). Nonetheless, the ACC results highlight the importance of zonal-track clusters for understanding extratropical forecast errors.

The experiments also suggest certain regions and model configurations are more prone to poor forecasts. In comparison with the forecasts for the US domain, the forecasts for Europe show lower ACCs (Figure 4a-d) and higher RMSE (Figure S7). For instance, the bottom quartiles of ACCs drop below 0.5 around Day 9 for Europe but around Day 12 for the US. Global maps also confirm that ACCs in Europe and its vicinity are the lowest in the Northern Hemisphere extratropics

(Figures S8–S10). The findings about Europe also hold in the deterministic NGCM experiments. Interestingly, Europe is the only region in the Northern Hemisphere extratropics where stochastic NGCM forecasts occasionally underperform their deterministic counterparts. Nonetheless, the stochastic NGCM forecasts outperform the deterministic NGCM on the global scale, suggesting that representing stochastic processes is critical for maintaining skill in challenging forecast scenarios.

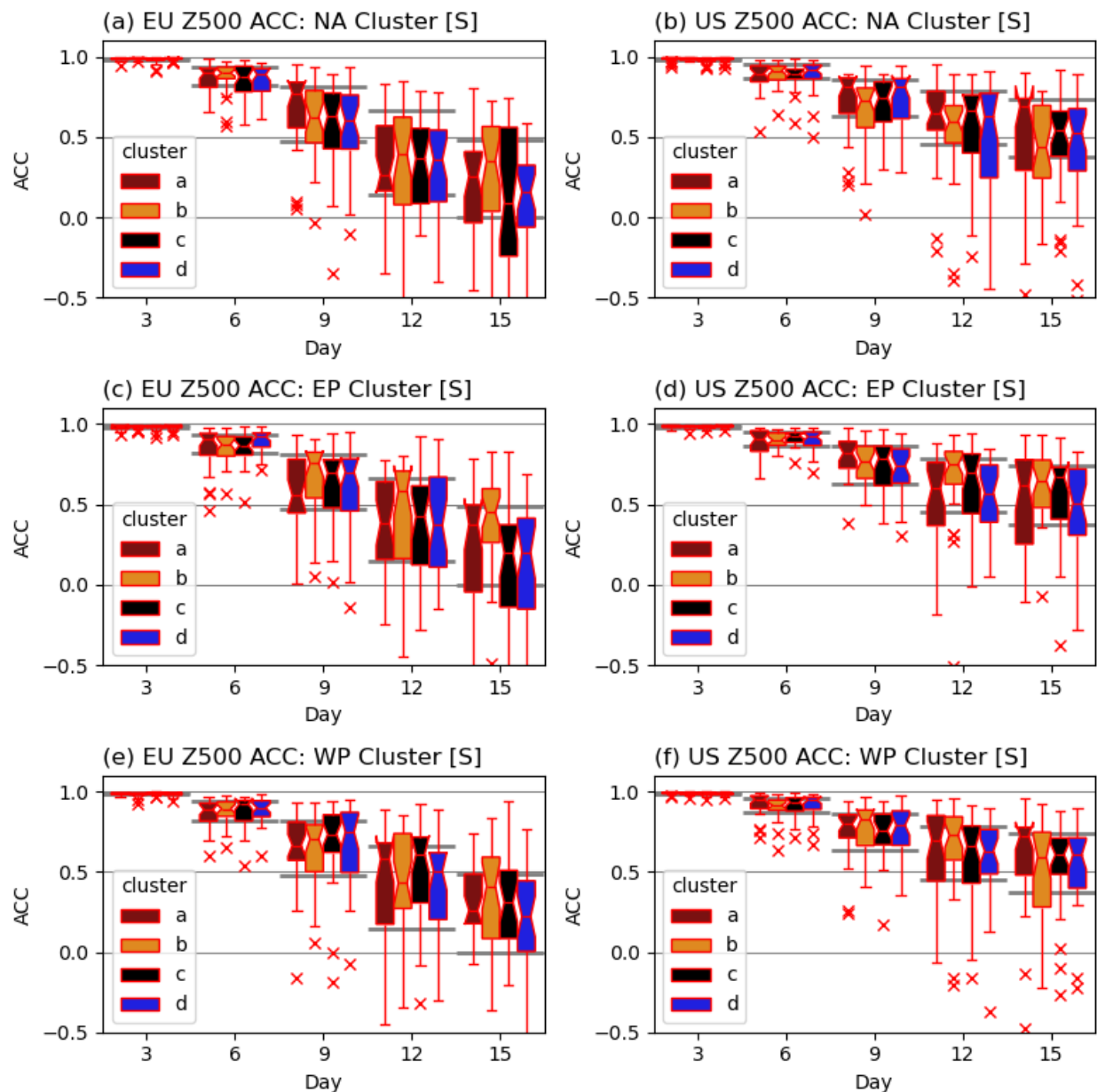


*Figure 4: Pattern ACCs of Z500 forecasts by the stochastic NGCM in the domains of Europe (left) and the US (right). (a) Pattern ACCs of the Europe domain ( $20^{\circ}\text{W}$ – $42.5^{\circ}\text{E}$ ,  $35$ – $75^{\circ}\text{N}$ ) for forecasts initialized near the genesis time of the North Atlantic tracks. The horizontal axis indicates the forecast lead days, and the vertical axis shows the ACCs. The box plots show the quartiles and the median of the ACCs, the 1.5 interquartile ranges (whiskers), and outliers (crosses) in each track cluster. The horizontal gray lines show the 25<sup>th</sup> and 75<sup>th</sup> percentile ranges of all the 359 forecast cases at each forecast lead. (b) Same as (a), but for pattern ACCs of the US domain ( $65$ – $128^{\circ}\text{W}$ ,  $20$ – $60^{\circ}\text{N}$ ). The Europe and US domains have the same number of grid points. (c-d) Same as (a-b), but for the East Pacific tracks. (e-f) Same as (a-b), but for the West Pacific tracks.*

## 5. Summary and Discussion

This study provides a systematic analysis using objective track clustering and comparative model forecasts (IFS and NGCM) to assess the impact of TCs on Northern Hemisphere extratropical forecasts out to 15 days. Our key conclusions are as follows:

1. Besides recurring TCs, some zonal track TCs can also contribute to large forecast errors. While recurring tracks that undergo extratropical transition contribute to high-amplitude errors (e.g., Hurricane Larry 2021), this study highlights that zonal-moving TCs can transport a high-volume of moisture to the midlatitudes and contribute to forecast error growth (e.g., Hurricane Laura 2020). Extremely low ACCs can occur in association with nearly all track clusters, highlighting the importance of zonal TC tracks for understanding extratropical forecast errors.
2. The high-resolution physics-based IFS and the lower-resolution hybrid NGCM make comparable predictions of the extratropical Z500 after TC genesis. Case studies show

qualitatively similar large-scale error growth patterns propagating downstream after TCs interact with the midlatitude flow in the IFS and the NGCM forecasts. When 102 cases are collectively evaluated, the two models have region-dependent but broadly comparable skill in the extratropics by Week 2. On the regional scale, the NGCM exhibits a skill deficit in the tropics but perform comparably in the NH extratropics relative to the IFS.

The model comparison also highlighted distinct AI model characteristics and development needs. Compared with the IFS, the NGCM systematically underperform near the initialization time and in the deep tropics (Figure 3b and 3d). These behaviors point towards potential challenges related to initialization shock and learned tropical convective processes on coarse grids (Figure 3b). This issue has been shared by the model developers and warrants further investigation. In Week-2 forecasts of extratropics, the stochastic NGCM performs comparably as the IFS (Figure 3 and S5-S6) and outperforms the deterministic NGCM (Figure S7–S10). The superior performance of the stochastic NGCM also likely benefits from its use of probabilistic training scoring, which helps improve the ensemble forecast performance of AI models with various architectures (Bonev et al., 2025; Kochkov et al., 2024; Lang et al., 2024). Overall, the findings underscore that for AI models, properly representing uncertainty in the initial conditions and physical processes is essential for maintaining robust skill, mirroring decades of development in traditional NWP.

Ultimately, this work underscores the profound and multifaceted impact of TC track characteristics on global weather predictability. It demonstrates that not only recurring tracks but also zonal tracks can severely degrade forecast skill. While the newly developed NGCM shows certain limitations (e.g., tropics), this study highlights its potential as a valuable tool for studying the large-scale flow predictability. A model intercomparison project that evaluate more physical and AI models will help verify the robustness of the findings and offer insights into forecast busts.

## Conflict of Interest

G.Z. holds stocks of Alphabet, which is the parent company of Google Research, the developer of NeuralGCM. G.Z. declares no other conflicts of interest for this manuscript.

## Acknowledgement

G.Z. thanks Dr. Janni Yuval for stimulating discussions about the NGCM and Ethan Cai for testing the track clustering algorithm. The research is supported by the U.S. National Science Foundation awards AGS-2327959 and RISE-2530555, as well as the faculty development fund of the University of Illinois Urbana-Champaign.

## Data Availability Statement

The NeuralGCM model and code are accessible at <https://neuralgcm.readthedocs.io/en/latest/>. The ERA5 data is available at: <https://console.cloud.google.com/marketplace/product/bigquery-public-data/arco-era5>. The TIGGE data is archived by ECMWF and available at: <https://apps.ecmwf.int/datasets/data/tigge/levtype=sfc/type=cf/>.

## References

Aiyyer, A. (2015). Recurving western North Pacific tropical cyclones and midlatitude predictability. *Geophysical Research Letters*, 42(18), 7799–7807.  
<https://doi.org/10.1002/2015GL065082>

Anwender, D., Harr, P. A., & Jones, S. C. (2008). Predictability Associated with the Downstream Impacts of the Extratropical Transition of Tropical Cyclones: Case Studies. *Monthly Weather Review*, 136(9), 3226–3247. <https://doi.org/10.1175/2008MWR2249.1>

Archambault, H. M., Bosart, L. F., Keyser, D., & Cordeira, J. M. (2013). A Climatological Analysis of the Extratropical Flow Response to Recurving Western North Pacific

Tropical Cyclones. *Monthly Weather Review*, 141(7), 2325–2346.

<https://doi.org/10.1175/MWR-D-12-00257.1>

Archambault, H. M., Keyser, D., Bosart, L. F., Davis, C. A., & Cordeira, J. M. (2015). A Composite Perspective of the Extratropical Flow Response to Recurring Western North Pacific Tropical Cyclones. *Monthly Weather Review*, 143(4), 1122–1141.

<https://doi.org/10.1175/MWR-D-14-00270.1>

Bauer, P., Thorpe, A., & Brunet, G. (2015). The quiet revolution of numerical weather prediction. *Nature*, 525(7567), 47–55. <https://doi.org/10.1038/nature14956>

Bi, K., Xie, L., Zhang, H., Chen, X., Gu, X., & Tian, Q. (2023). Accurate medium-range global weather forecasting with 3D neural networks. *Nature*, 619(7970), 533–538.

<https://doi.org/10.1038/s41586-023-06185-3>

Bonev, B., Kurth, T., Mahesh, A., Bisson, M., Kossaifi, J., Kashinath, K., et al. (2025). FourCastNet 3: A geometric approach to probabilistic machine-learning weather forecasting at scale (Version 2). arXiv. <https://doi.org/10.48550/ARXIV.2507.12144>

Bosart, L. F., Cordeira, J. M., Galarneau, T. J., Moore, B. J., & Archambault, H. M. (2012). An Analysis of Multiple Predecessor Rain Events ahead of Tropical Cyclones Ike and Lowell: 10–15 September 2008. *Monthly Weather Review*, 140(4), 1081–1107.

<https://doi.org/10.1175/MWR-D-11-00163.1>

Bougeault, P., Toth, Z., Bishop, C., Brown, B., Burridge, D., Chen, D. H., et al. (2010). The THORPEX Interactive Grand Global Ensemble. *Bulletin of the American Meteorological Society*, 91(8), 1059–1072. <https://doi.org/10.1175/2010BAMS2853.1>

Brannan, A. L., & Chagnon, J. M. (2020). A Climatology of the Extratropical Flow Response to Recurving Atlantic Tropical Cyclones. *Monthly Weather Review*, 148(2), 541–558. <https://doi.org/10.1175/MWR-D-19-0216.1>

Camargo, S. J., Robertson, A. W., Gaffney, S. J., Smyth, P., & Ghil, M. (2007). Cluster Analysis of Typhoon Tracks. Part I: General Properties. *Journal of Climate*, 20(14), 3635–3653. <https://doi.org/10.1175/JCLI4188.1>

Camargo, S. J., Robertson, A. W., Barnston, A. G., & Ghil, M. (2008). Clustering of eastern North Pacific tropical cyclone tracks: ENSO and MJO effects. *Geochemistry, Geophysics, Geosystems*, 9(6), 2007GC001861. <https://doi.org/10.1029/2007GC001861>

Camargo, S. J., Vitart, F., Lee, C.-Y., & Tippett, M. K. (2021). Skill, Predictability, and Cluster Analysis of Atlantic Tropical Storms and Hurricanes in the ECMWF Monthly Forecasts. *Monthly Weather Review*, 149(11), 3781–3802. <https://doi.org/10.1175/MWR-D-21-0075.1>

Chen, Z., Leung, L. R., Zhou, W., Lu, J., Lubis, S. W., Liu, Y., et al. (2025, October 19). Hierarchical Testing of a Hybrid Machine Learning-Physics Global Atmosphere Model. Preprints. <https://doi.org/10.22541/essoar.176083829.92588794/v1>

Cordeira, J. M., Ralph, F. M., & Moore, B. J. (2013). The Development and Evolution of Two Atmospheric Rivers in Proximity to Western North Pacific Tropical Cyclones in October 2010. *Monthly Weather Review*, 141(12), 4234–4255. <https://doi.org/10.1175/MWR-D-13-00019.1>

DelSole, T., & Tippett, M. K. (2016). Forecast Comparison Based on Random Walks. *Monthly Weather Review*, 144(2), 615–626. <https://doi.org/10.1175/MWR-D-15-0218.1>

DeMaria, M., Franklin, J. L., Chirokova, G., Radford, J., DeMaria, R., Musgrave, K. D., & Ebert-Uphoff, I. (2025). An Operations-Based Evaluation of Tropical Cyclone Track and Intensity Forecasts from Artificial Intelligence Weather Prediction Models. *Artificial Intelligence for the Earth Systems*, 4(4), 240085. <https://doi.org/10.1175/AIES-D-24-0085.1>

Evans, C., Wood, K. M., Aberson, S. D., Archambault, H. M., Milrad, S. M., Bosart, L. F., et al. (2017). The Extratropical Transition of Tropical Cyclones. Part I: Cyclone Evolution and Direct Impacts. *Monthly Weather Review*, 145(11), 4317–4344. <https://doi.org/10.1175/MWR-D-17-0027.1>

Galarneau, T. J., Bosart, L. F., & Schumacher, R. S. (2010). Predecessor Rain Events ahead of Tropical Cyclones. *Monthly Weather Review*, 138(8), 3272–3297. <https://doi.org/10.1175/2010MWR3243.1>

Grams, C. M., & Archambault, H. M. (2016). The Key Role of Diabatic Outflow in Amplifying the Midlatitude Flow: A Representative Case Study of Weather Systems Surrounding Western North Pacific Extratropical Transition. *Monthly Weather Review*, 144(10), 3847–3869. <https://doi.org/10.1175/MWR-D-15-0419.1>

Hakim, G. J., & Masanam, S. (2023). Dynamical Tests of a Deep-Learning Weather Prediction Model (Version 1). <https://doi.org/10.48550/ARXIV.2309.10867>

Han, Y., & Ullrich, P. A. (2025). The System for Classification of Low-Pressure Systems (SyCLOPS): An All-In-One Objective Framework for Large-Scale Data Sets. *Journal of Geophysical Research: Atmospheres*, 130(1), e2024JD041287. <https://doi.org/10.1029/2024JD041287>

Harr, P., & Archambault, H. (2017). The Impacts of Recurring Tropical Cyclone on Extended-Range Predictability of Midlatitude Weather Patterns. Presented at the 97th American Meteorological Society Annual Meeting, Seattle, WA. Retrieved from <https://ams.confex.com/ams/97Annual/webprogram/Paper312097.html>

Hersbach, H., Bell, B., Berrisford, P., Hirahara, S., Horányi, A., Muñoz-Sabater, J., et al. (2020). The ERA5 global reanalysis. *Quarterly Journal of the Royal Meteorological Society*, 146(730), 1999–2049. <https://doi.org/10.1002/qj.3803>

Hodges, K., Cobb, A., & Vidale, P. L. (2017). How Well Are Tropical Cyclones Represented in Reanalysis Datasets? *Journal of Climate*, 30(14), 5243–5264. <https://doi.org/10.1175/JCLI-D-16-0557.1>

Keller, J. H., Grams, C. M., Riemer, M., Archambault, H. M., Bosart, L., Doyle, J. D., et al. (2019). The Extratropical Transition of Tropical Cyclones. Part II: Interaction with the Midlatitude Flow, Downstream Impacts, and Implications for Predictability. *Monthly Weather Review*, 147(4), 1077–1106. <https://doi.org/10.1175/MWR-D-17-0329.1>

Knapp, K. R., Kruk, M. C., Levinson, D. H., Diamond, H. J., & Neumann, C. J. (2010). The International Best Track Archive for Climate Stewardship (IBTrACS): Unifying Tropical Cyclone Data. *Bulletin of the American Meteorological Society*, 91(3), 363–376. <https://doi.org/10.1175/2009BAMS2755.1>

Kochkov, D., Yuval, J., Langmore, I., Norgaard, P., Smith, J., Mooers, G., et al. (2024). Neural general circulation models for weather and climate. *Nature*. <https://doi.org/10.1038/s41586-024-07744-y>

Kossin, J. P., Camargo, S. J., & Sitkowski, M. (2010). Climate Modulation of North Atlantic Hurricane Tracks. *Journal of Climate*, 23(11), 3057–3076.  
<https://doi.org/10.1175/2010JCLI3497.1>

Lam, R., Sanchez-Gonzalez, A., Willson, M., Wirnsberger, P., Fortunato, M., Alet, F., et al. (2023). Learning skillful medium-range global weather forecasting. *Science*, 382(6677), 1416–1421. <https://doi.org/10.1126/science.adi2336>

Lang, S., Alexe, M., Clare, M. C. A., Roberts, C., Adewoyin, R., Bouallègue, Z. B., et al. (2024). AIFS-CRPS: Ensemble forecasting using a model trained with a loss function based on the Continuous Ranked Probability Score (Version 1). arXiv.  
<https://doi.org/10.48550/ARXIV.2412.15832>

Lee, J.-G., Han, J., & Whang, K.-Y. (2007). Trajectory clustering: a partition-and-group framework. In *Proceedings of the 2007 ACM SIGMOD international conference on Management of data* (pp. 593–604). Beijing China: ACM.  
<https://doi.org/10.1145/1247480.1247546>

Lillo, S. P., & Parsons, D. B. (2017). Investigating the dynamics of error growth in ECMWF medium-range forecast busts. *Quarterly Journal of the Royal Meteorological Society*, 143(704), 1211–1226. <https://doi.org/10.1002/qj.2938>

Pasche, O. C., Wider, J., Zhang, Z., Zscheischler, J., & Engelke, S. (2025). Validating Deep Learning Weather Forecast Models on Recent High-Impact Extreme Events. *Artificial Intelligence for the Earth Systems*, 4(1), e240033. <https://doi.org/10.1175/AIES-D-24-0033.1>

Pohorsky, R., Röthlisberger, M., Grams, C. M., Riboldi, J., & Martius, O. (2019). The Climatological Impact of Recurring North Atlantic Tropical Cyclones on Downstream

Extreme Precipitation Events. *Monthly Weather Review*, 147(5), 1513–1532.

<https://doi.org/10.1175/MWR-D-18-0195.1>

Price, I., Sanchez-Gonzalez, A., Alet, F., Ewalds, T., El-Kadi, A., Stott, J., et al. (2023). GenCast:

Diffusion-based ensemble forecasting for medium-range weather (Version 1).

<https://doi.org/10.48550/ARXIV.2312.15796>

Quinting, J. F., & Jones, S. C. (2016). On the Impact of Tropical Cyclones on Rossby Wave

Packets: A Climatological Perspective. *Monthly Weather Review*, 144(5), 2021–2048.

<https://doi.org/10.1175/MWR-D-14-00298.1>

Riboldi, J., Grams, C. M., Riemer, M., & Archambault, H. M. (2019). A Phase Locking

Perspective on Rossby Wave Amplification and Atmospheric Blocking Downstream of

Recurving Western North Pacific Tropical Cyclones. *Monthly Weather Review*, 147(2),

567–589. <https://doi.org/10.1175/MWR-D-18-0271.1>

Riemer, M., & Jones, S. C. (2010). The downstream impact of tropical cyclones on a developing

baroclinic wave in idealized scenarios of extratropical transition. *Quarterly Journal of the*

*Royal Meteorological Society*, 136(648), 617–637. <https://doi.org/10.1002/qj.605>

Riemer, M., & Jones, S. C. (2014). Interaction of a tropical cyclone with a high-amplitude,

midlatitude wave pattern: Waviness analysis, trough deformation and track bifurcation.

*Quarterly Journal of the Royal Meteorological Society*, 140(681), 1362–1376.

<https://doi.org/10.1002/qj.2221>

Rodwell, M. J., Magnusson, L., Bauer, P., Bechtold, P., Bonavita, M., Cardinali, C., et al. (2013).

Characteristics of Occasional Poor Medium-Range Weather Forecasts for Europe.

*Bulletin of the American Meteorological Society*, 94(9), 1393–1405.

<https://doi.org/10.1175/BAMS-D-12-00099.1>

Sinclair, M. R. (2025). A Global Climatology of Tropical Cyclone Diabatic Rossby Wave Sources and their Extratropical Flow Response. *Journal of Climate*, e250175. <https://doi.org/10.1175/JCLI-D-25-0175.1>

Takaya, K., & Nakamura, H. (2001). A Formulation of a Phase-Independent Wave-Activity Flux for Stationary and Migratory Quasigeostrophic Eddies on a Zonally Varying Basic Flow. *Journal of the Atmospheric Sciences*, 58(6), 608–627. [https://doi.org/10.1175/1520-0469\(2001\)058%3C0608:AFOAPI%3E2.0.CO;2](https://doi.org/10.1175/1520-0469(2001)058%3C0608:AFOAPI%3E2.0.CO;2)

Ullrich, P. A., Zarzycki, C. M., McClenny, E. E., Pinheiro, M. C., Stansfield, A. M., & Reed, K. A. (2021). TempestExtremes v2.1: a community framework for feature detection, tracking, and analysis in large datasets. *Geoscientific Model Development*, 14(8), 5023–5048. <https://doi.org/10.5194/gmd-14-5023-2021>

Zhang, G., Wang, Z., Dunkerton, T. J., Peng, M. S., & Magnusdottir, G. (2016). Extratropical Impacts on Atlantic Tropical Cyclone Activity. *Journal of the Atmospheric Sciences*, 73(3), 1401–1418. <https://doi.org/10.1175/JAS-D-15-0154.1>

Zhang, G., Wang, Z., Peng, M. S., & Magnusdottir, G. (2017). Characteristics and Impacts of Extratropical Rossby Wave Breaking during the Atlantic Hurricane Season. *Journal of Climate*, 30(7), 2363–2379. <https://doi.org/10.1175/JCLI-D-16-0425.1>

Zhang, G., Rao, M., Yuval, J., & Zhao, M. (2025). Advancing seasonal prediction of tropical cyclone activity with a hybrid AI-physics climate model. *Environmental Research Letters*, 20(9), 094031. <https://doi.org/10.1088/1748-9326/adf864>

Supplementary Materials

for

**Linking Extratropical Forecast Degradation to Tropical Cyclones in Physical  
and AI Models**

**Gan Zhang<sup>1\*</sup>**

<sup>1</sup> Department of Climate, Meteorology & Atmospheric Sciences, University of Illinois at Urbana-Champaign, Urbana, Illinois

\*Corresponding Author: Gan Zhang (gzhang13@illinois.edu)

File Content

- Supplementary Discussion
- Figures S1–S10

## Parameter Choice of K-means Clustering

We conducted sensitivity tests of the k-means track clustering using a range of k values. Figure S1 shows the results of k = 3, 4, 5, and 6 for the North Atlantic tracks. The results suggest the algorithm clusters tracks based on genesis locations and TC tracks. When k value increases, track clusters show more granular regional splitting. The results indicate that k=4 provides a meaningful separation into geographically distinct archetypes (e.g., primarily zonal vs. recurving tracks) relevant to potential TC-midlatitude interactions. Furthermore, k = 4 prevents over small cluster sample sizes that makes it challenging to conduct inter-cluster comparison of forecast skills. We also note that previous studies of the North Atlantic TC tracks also use four clusters (e.g., Camargo et al., 2007, 2008; Kossin et al., 2010), which produces some similar track clusters. The k values were evaluated for other basins, and more details are available in the code repository (Data Availability).

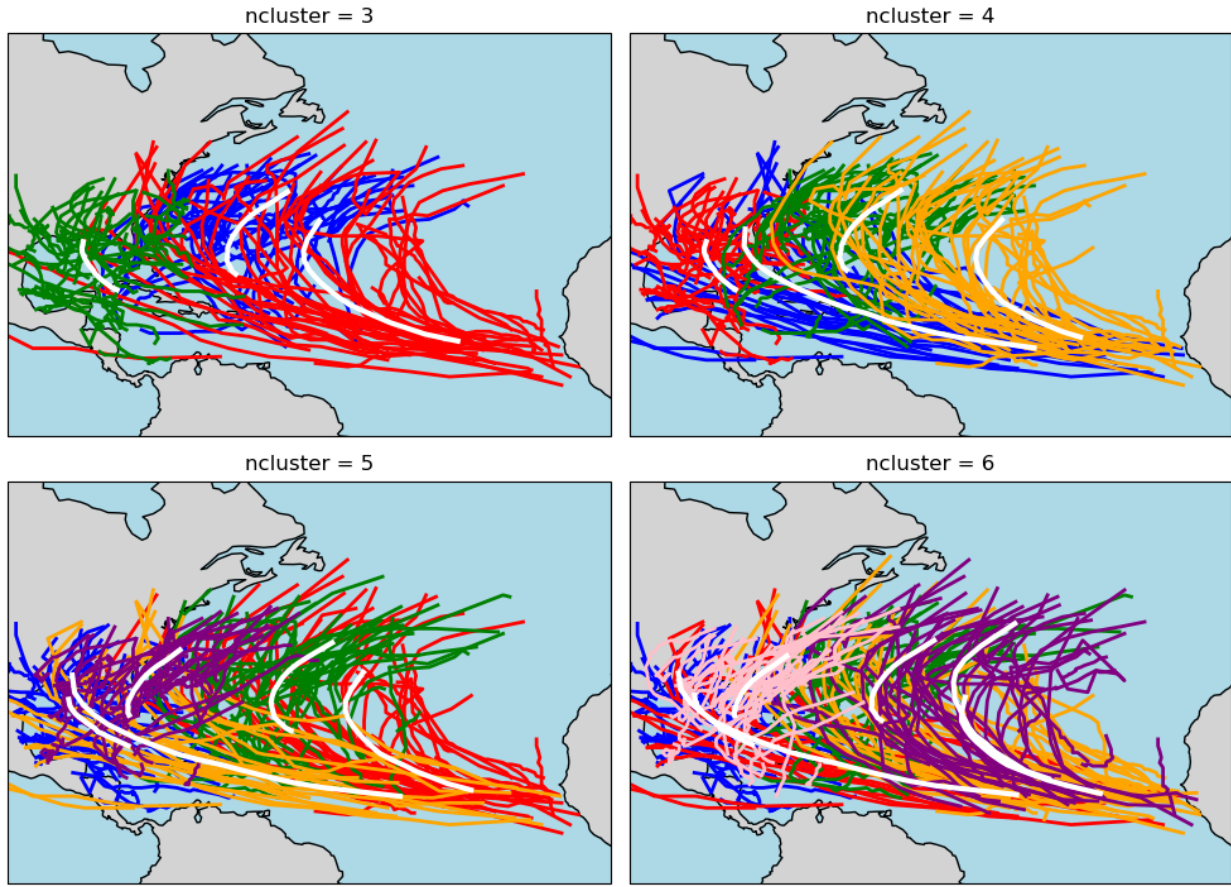


*Figure S1: An example showing North Atlantic track clusters with  $k = 3, 4, 5$ , and  $6$ . Individual tracks in each cluster are marked with different colors. Thickened white lines with black edges indicate mean trajectories of all tracks in each cluster.*

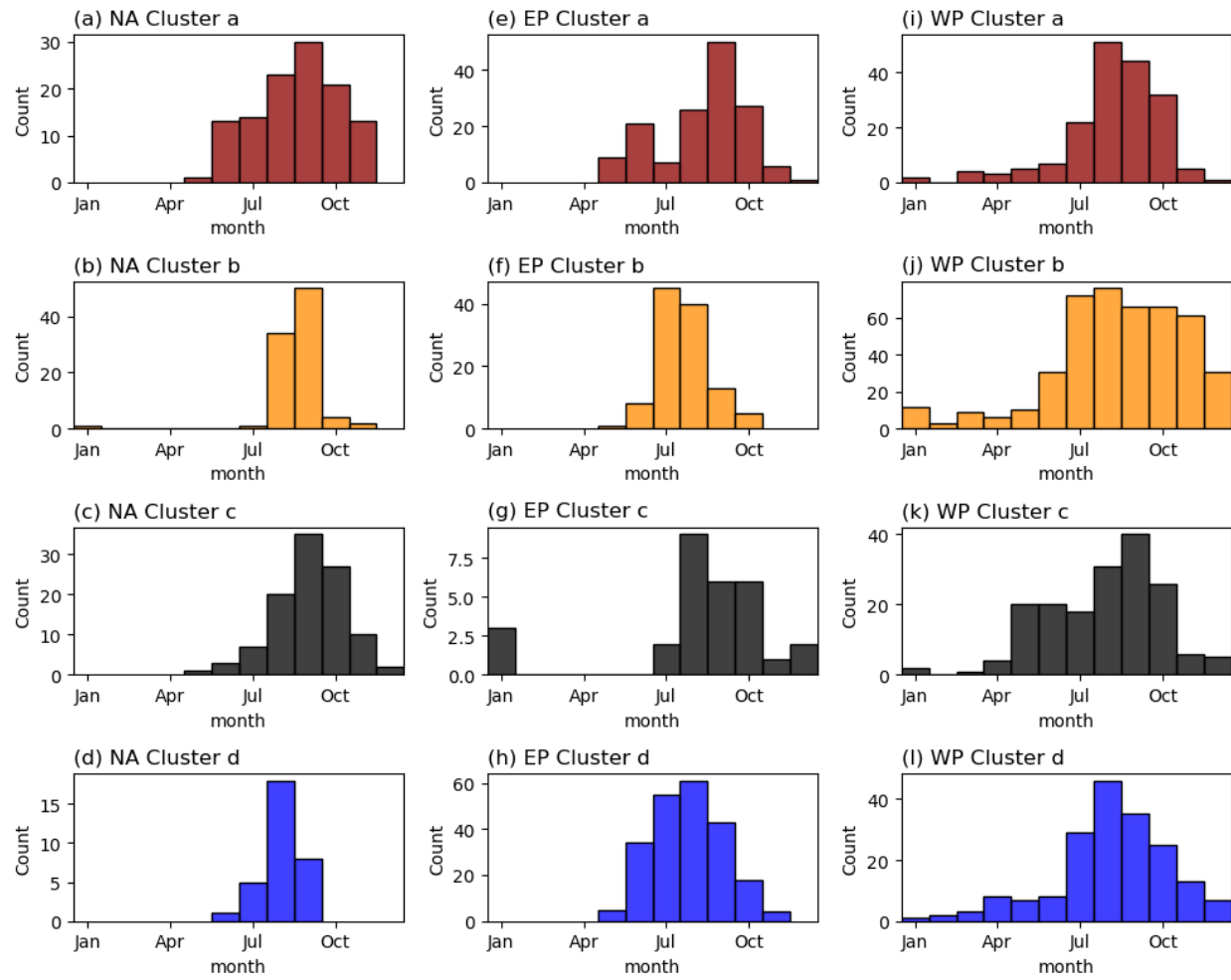
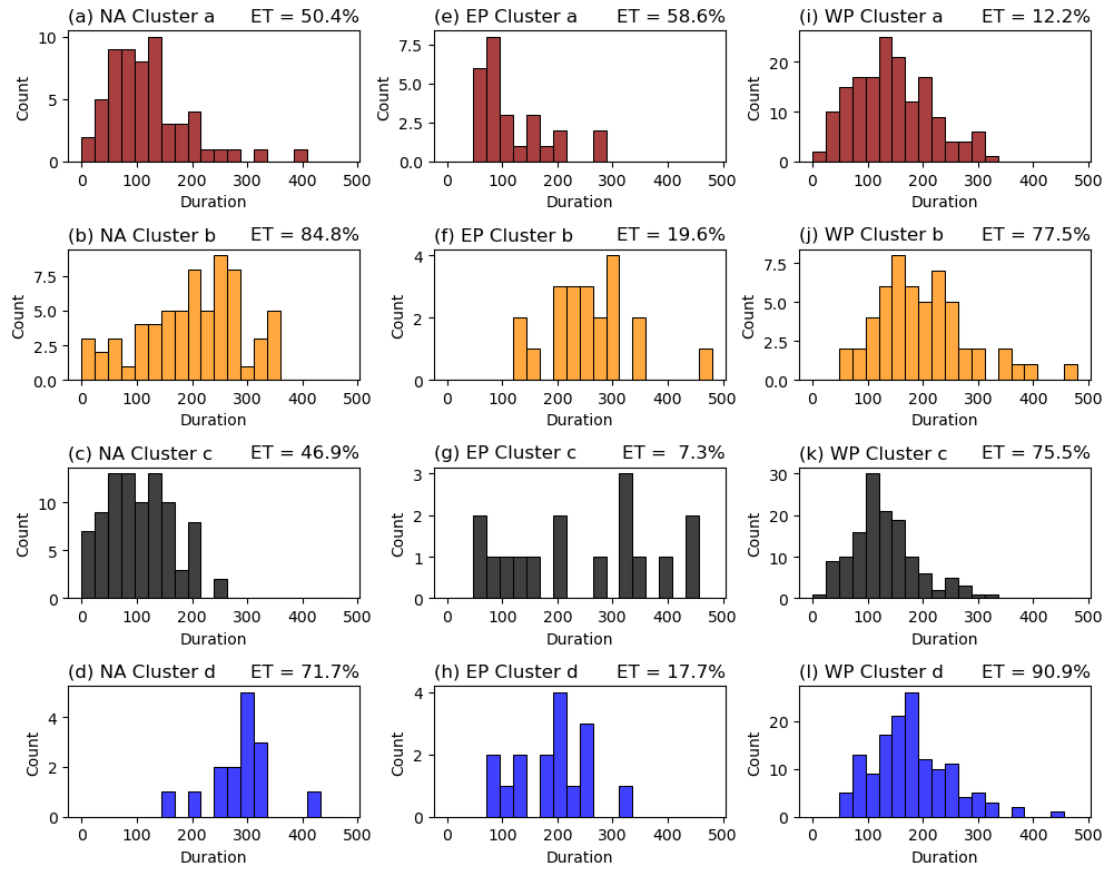
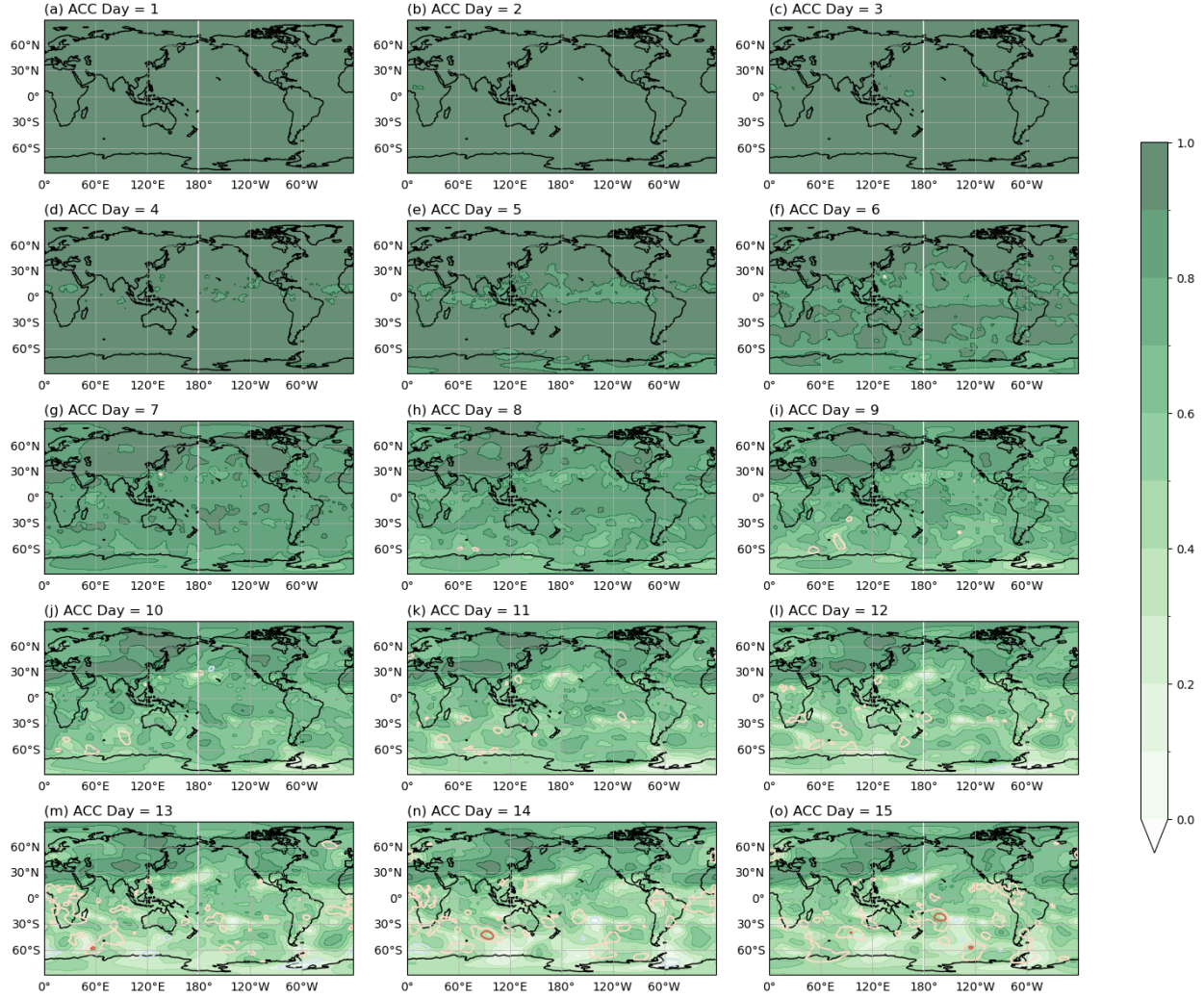


Figure S2: Monthly distributions of genesis time for each TC cluster in (a-d) the North Atlantic (NA), (e-h) Eastern Pacific (EP), and (i-l) Western Pacific (WP) basins.



*Figure S3: Duration (hour) distributions for each TC cluster in (a-d) the North Atlantic (NA), (e-h) Eastern Pacific (EP), and (i-l) Western Pacific (WP) basins. The ratio of the extratropical transition (ET) percentages is calculated for each cluster and denoted in the top right of each panel.*



*Figure S4: Skill of IFS Z500 forecasts (ACC) for 102 cases during 2020-2022. Panels (a-o) show forecast skill for the lead time of Day 1 to Day 15, respectively. The forecasts are initialized around the genesis time (Methods). Shading represents the ACC values of a 20-member ensemble, while contours denote the difference between the 50-member ensemble and the 20-member ensemble. The contour level interval of ACC difference is 0.05, with zero contour line omitted for clarity. Smaller ACC values indicate less skillful predictions.*

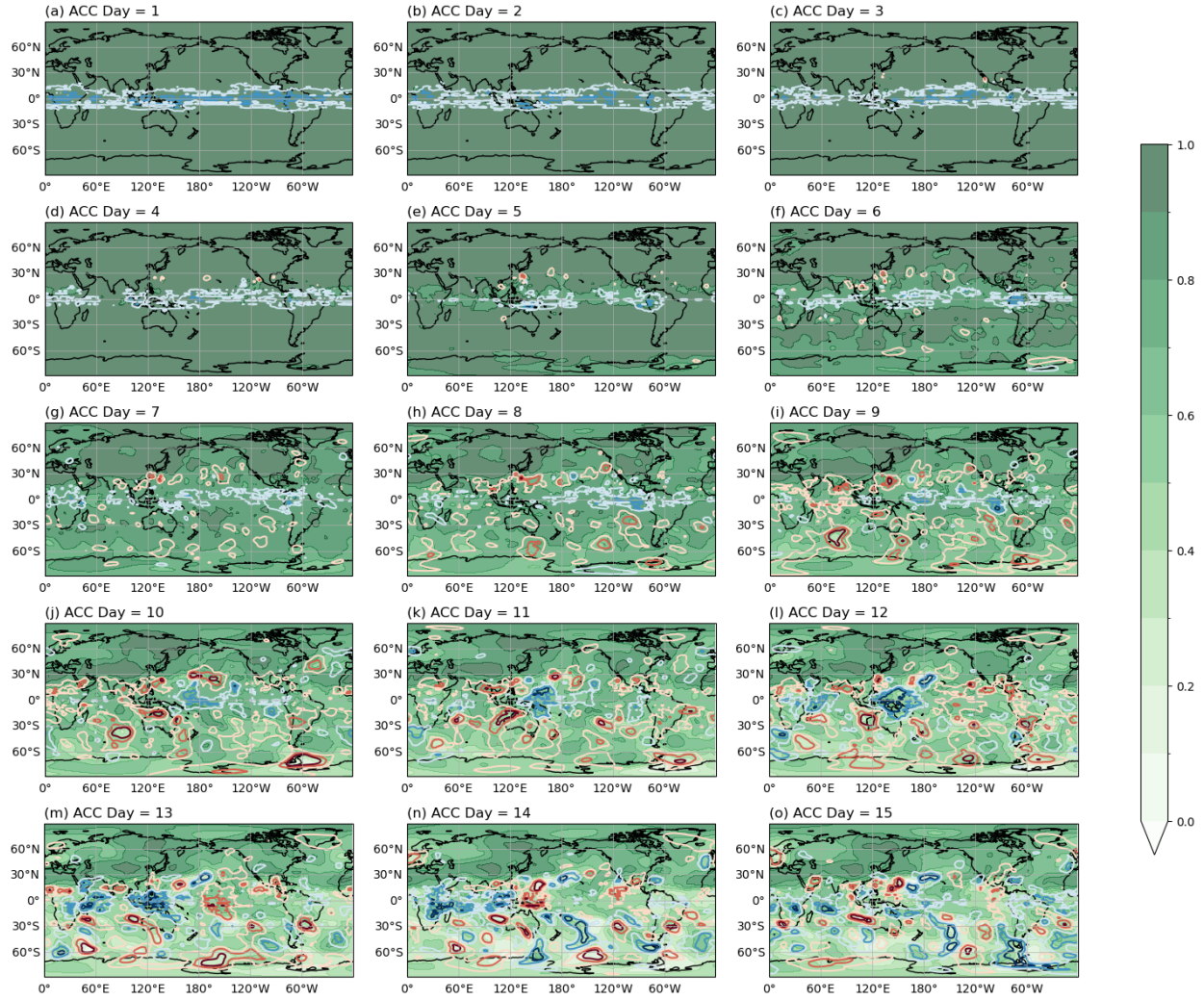


*Figure S5: Differences (contours) between the NGCM and the IFS skill of Z500 forecasts (ACC) for 102 cases during 2020-2022. The NGCM forecast skill is calculated using a 20-member ensemble of the stochastic NGCM. The other plotting settings are the same as Figure S4. Smaller ACC values indicate less skillful predictions.*

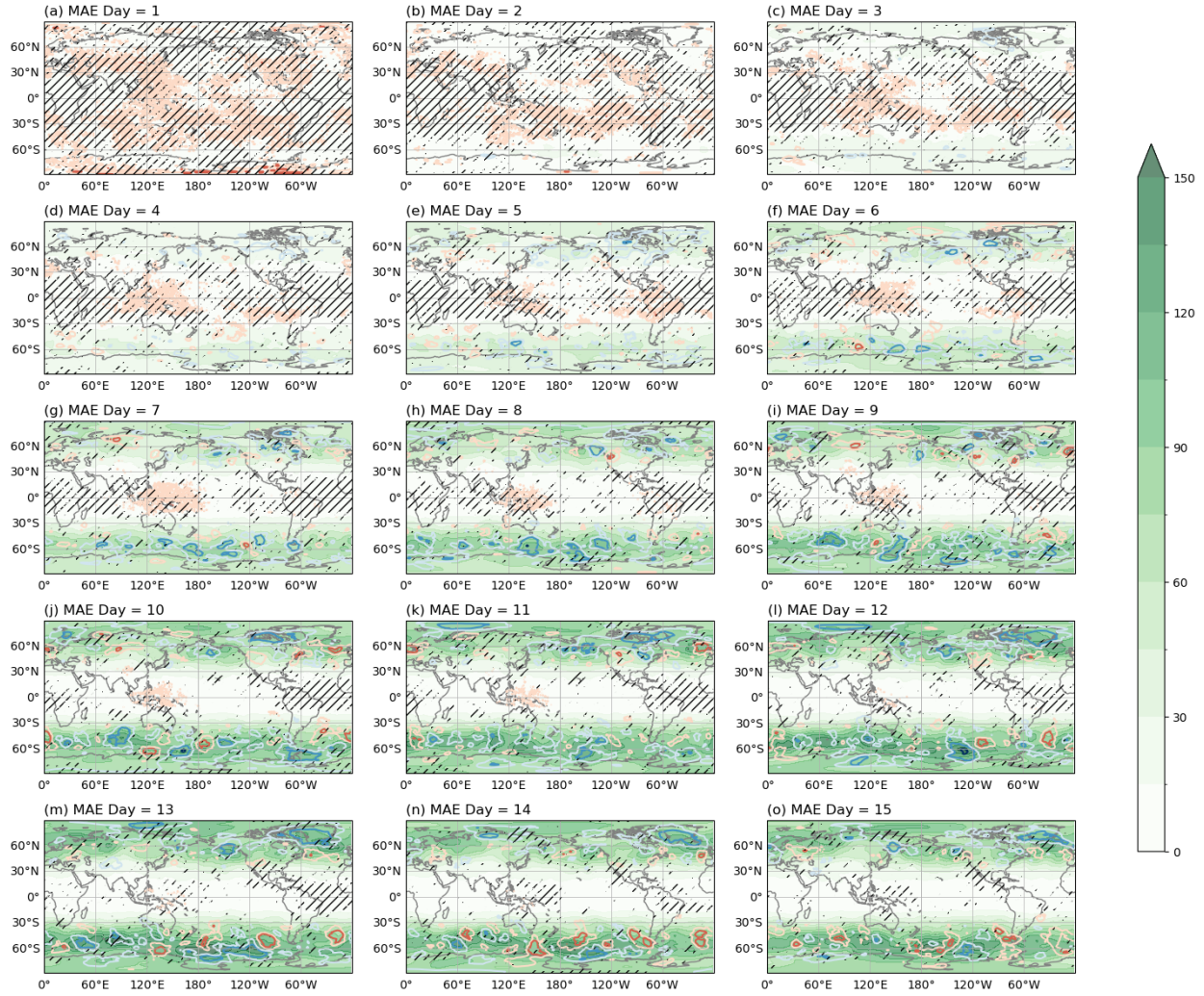


*Figure S6: Same as Figure S5, but for the mean absolute error (MAE). The contour levels of MAE differences are -20, -10, -5, 5, 10, 20 m. Hatching highlight the regions where IFS and NGCM are different at the 90%-confidence level, indicated by a sign test (DelSole & Tippett, 2016). Larger MAE values indicate less skillful predictions.*

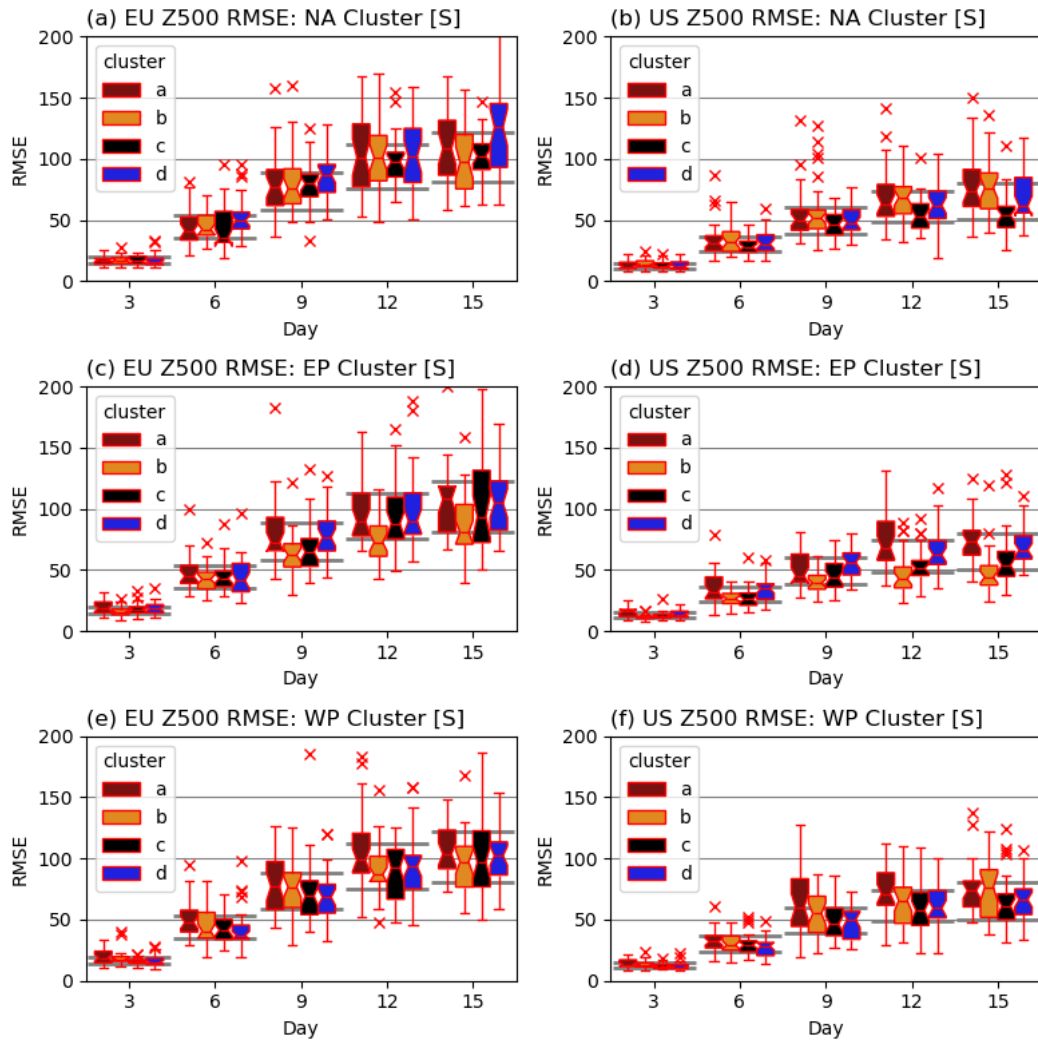
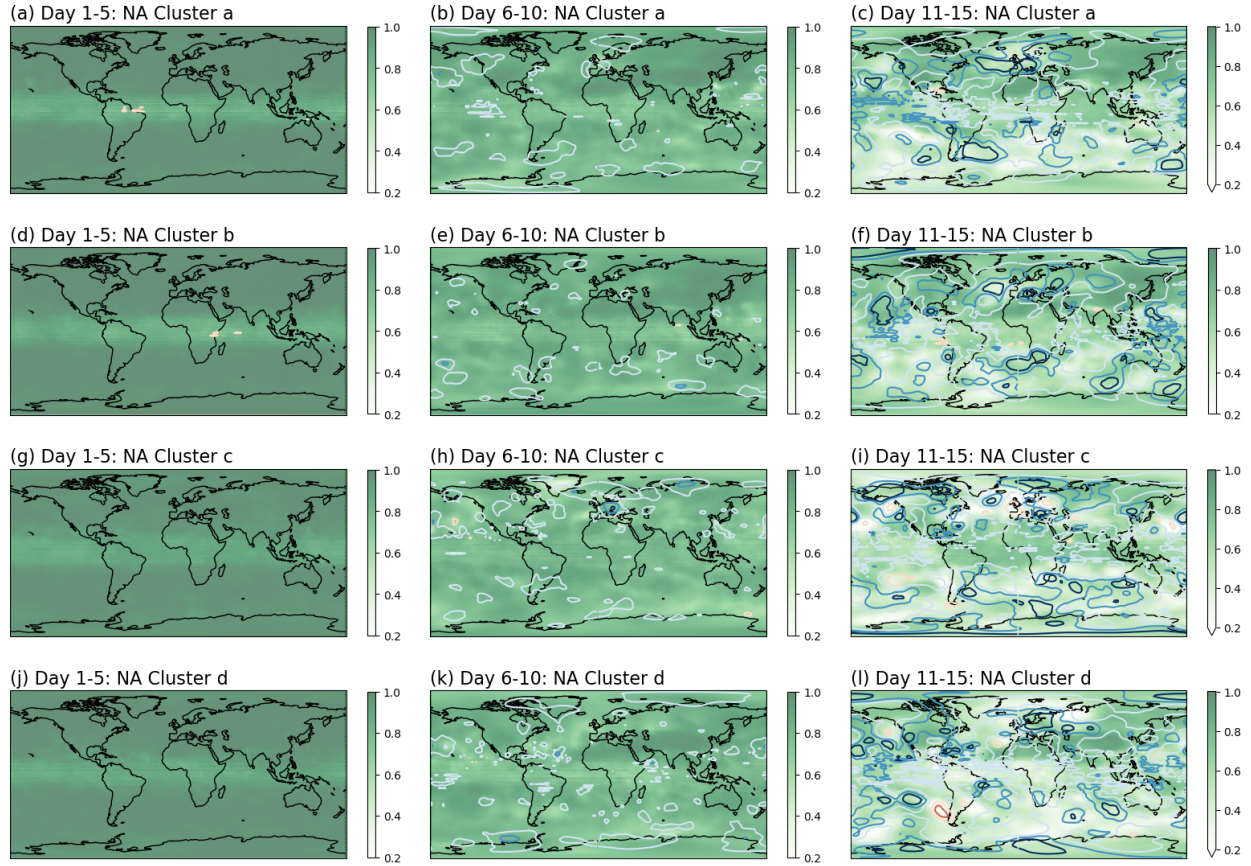


Figure S7: Same as Figure 4, but for the RMSE.



*Figure S8: Five-day mean skill of NGCM forecasts for each track cluster in the North Atlantic. Shading shows the ACC of 500-hPa geopotential height of the 20-member stochastic forecasts. Contours show the skill differences between the deterministic NGCM and the stochastic NGCM. The contour level interval of ACC difference is 0.1, with zero contour line omitted for clarity. (a-c) Mean ACC for the forecasts of track cluster a averaged over Day 1-5, 6-10, and 11-15, respectively. (d-f), (g-i), and (j-l): Same as (a-c), but for clusters b, c, and d. The calculations used the anomalies defined using the averages of the 102 cases during 2020-2022 for each forecast dataset.*

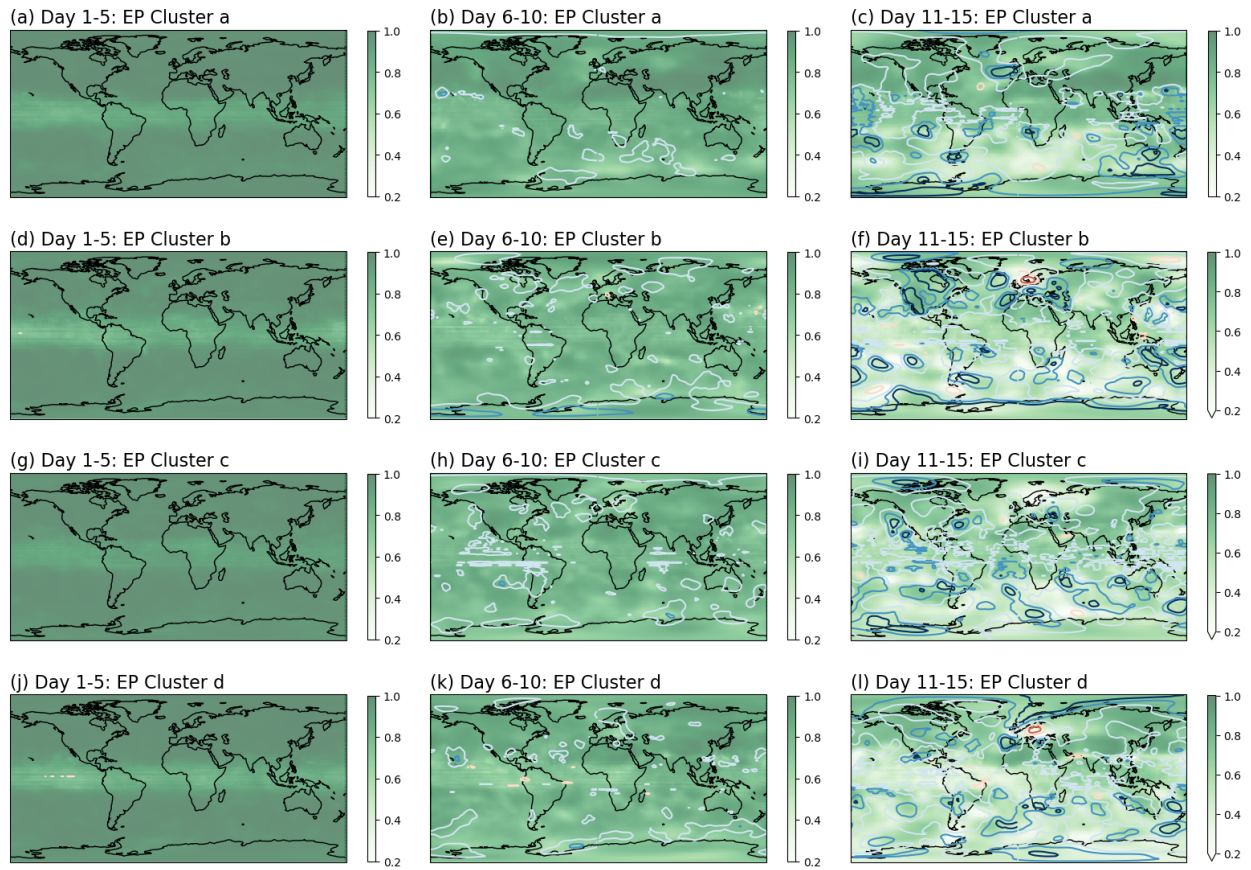


Figure S9: Same as Figure S8, but for the Northeast Pacific clusters.

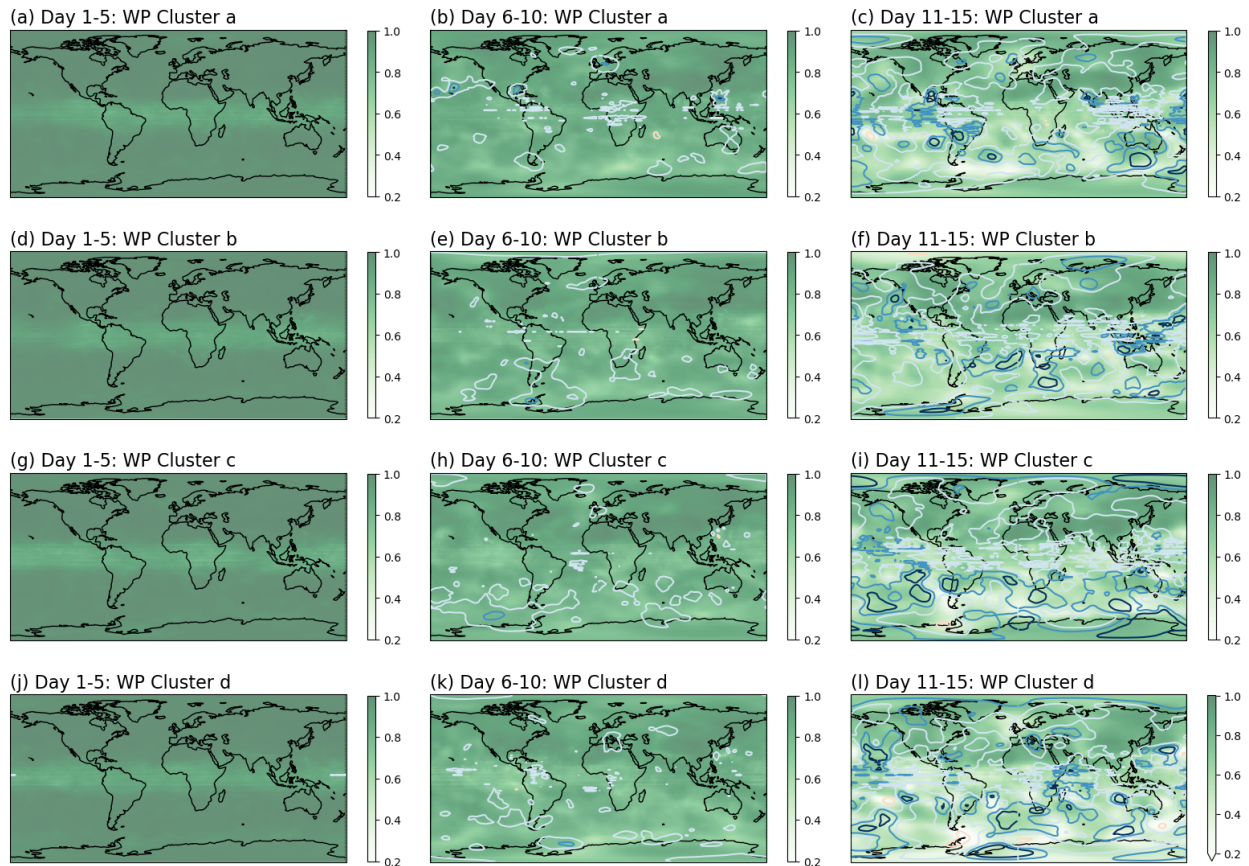


Figure S10: Same as Figure S8, but for the Northwest Pacific track clusters.